


## AUTHOR QUERY FORM

 <b>ELSEVIER</b>	<b>Journal: YJTBI</b> <b>Article Number: 6545</b>	<b>Please e-mail or fax your responses and any corrections to:</b> <b>E-mail: <a href="mailto:corrections.essd@elsevier.macipd.com">corrections.essd@elsevier.macipd.com</a></b> <b>Fax: +44 1392 285878</b>
--	--	--

Dear Author,

Please check your proof carefully and mark all corrections at the appropriate place in the proof (e.g., by using on-screen annotation in the PDF file) or compile them in a separate list.

For correction or revision of any artwork, please consult <http://www.elsevier.com/artworkinstructions>.

Any queries or remarks that have arisen during the processing of your manuscript are listed below and highlighted by flags in the proof. Click on the [Q](#) link to go to the location in the proof.

Location in article	Query / Remark: <a href="#">click on the Q link to go</a> Please insert your reply or correction at the corresponding line in the proof
<a href="#">Q1</a>	Reference(s) given here were noted in the reference list but are missing from the text – please position each reference in the text or delete it from the list.
<a href="#">Q2</a>	Please note that the reference style has been changed from a Numbered style to a Name-Date style as per the journal specifications.
<a href="#">Q3</a>	Fig. 3 has been submitted as color image; however, the caption has been reworded to ensure that it is meaningful when your article is reproduced both in color and in black and white. Please check and correct if necessary

Thank you for your assistance.



ELSEVIER

Contents lists available at ScienceDirect

## Journal of Theoretical Biology

journal homepage: [www.elsevier.com/locate/jtbi](http://www.elsevier.com/locate/jtbi)

## Highlights

**How to assess, visualize and compare the anisotropy of linear structures reconstructed from optical sections—A study based on histopathological quantification of human brain microvessels**

Journal of Theoretical Biology ■ (■■■■) ■■■–■■■

Petra Kochová<sup>a</sup>, Robert Cimrman<sup>a</sup>, Jiří Janáček<sup>b</sup>, Kirsti Witter<sup>c</sup>, Zbyněk Tonar<sup>d,e</sup><sup>a</sup> Department of Mechanics, Faculty of Applied Sciences, University of West Bohemia, Univerzitní 8, 306 14 Pilsen, Czech Republic<sup>b</sup> Institute of Physiology, Academy of Sciences of the Czech Republic, Vídeňská 1083, 142 20 Prague, Czech Republic

► We present  $p(\chi\text{-square})$  method for evaluating anisotropy of linear systems. ► We compared this novel method with ellipsoidal and fractional anisotropy. ► We determined preferential directions and anisotropy of brain blood microvessels. ► Microvessels in cortex were more anisotropic than in white matter. ► We created open source software (esofspy) to calculate measures of anisotropy.



Contents lists available at ScienceDirect

Journal of Theoretical Biology

journal homepage: [www.elsevier.com/locate/yjtbi](http://www.elsevier.com/locate/yjtbi)

# How to assess, visualize and compare the anisotropy of linear structures reconstructed from optical sections—A study based on histopathological quantification of human brain microvessels

Petra Kochová<sup>a,\*</sup>, Robert Cimrman<sup>a</sup>, Jiří Janáček<sup>b</sup>, Kirsti Witter<sup>c</sup>, Zbyněk Tonar<sup>d,e</sup>

<sup>a</sup> Department of Mechanics, Faculty of Applied Sciences, University of West Bohemia, Univerzitní 8, 306 14 Pilsen, Czech Republic

<sup>b</sup> Institute of Physiology, Academy of Sciences of the Czech Republic, Vídeňská 1083, 142 20 Prague, Czech Republic

<sup>c</sup> Institute of Anatomy, Histology and Embryology, Department for Pathobiology, University of Veterinary Medicine Vienna, Veterinärplatz 1, A-1210 Vienna, Austria

<sup>d</sup> European Centre of Excellence NTIS—New Technologies for Information Society, Faculty of Applied Sciences, University of West Bohemia, Univerzitní 22, 306 14 Pilsen, Czech Republic

<sup>e</sup> Department of Histology and Embryology, Faculty of Medicine in Pilsen, Charles University in Prague, Karlovarská 48, 301 66 Pilsen, Czech Republic

## ARTICLE INFO

### Article history:

Received 16 December 2010

Received in revised form

1 July 2011

Accepted 6 July 2011

### Keywords:

Rose of directions

Preferential directions

Chi-square test

Length density

Python

## ABSTRACT

Three-dimensional analyses of the spatial arrangement, spatial orientation and preferential directions of systems of fibers are frequent tasks in many scientific fields, including the textile industry, plant biology and tissue modeling. In biology, systems of oriented and branching lines are often used to represent the three-dimensional directionality and topology of microscopic blood vessels supplying various organs. In our study, we present a novel  $p(\chi^2)$  (chi-square) method for evaluating the anisotropy of line systems that involves comparing the observed length densities of lines with the discrete uniform distribution of an isotropic line system with the  $\chi^2$ -test. Using this method in our open source software, we determined the rose of directions, preferential directions and level of anisotropy of linear systems representing the microscopic blood vessels in samples of various regions from human brains (cortex, subcortical gray matter and white matter). The novel method was compared with two other methods used for anisotropy quantification (ellipsoidal and fractional anisotropy). All three methods detected different levels of anisotropy of blood microvessels in human brain. The microvascular bed in the cortex was closer to an isotropic network, while the microvessels supplying the white matter appeared to be an anisotropic and direction-sensitive system. All three methods were able to determine the differences between various brain regions. The advantage of our  $p(\chi^2)$  method is its high correlation with the number of preferential directions of the line system. However, the software, named esofspy, is able to calculate all three of the measures of anisotropy compared and documented in this paper, thus making the methods freely available to the scientific community.

© 2011 Elsevier Ltd. All rights reserved.

## 1. Introduction

Cerebral circulation is fundamental to health and the maintenance of brain tissue (Monson et al., 2008; Schlimper et al., 2010). Recently, modern imaging methods, such as different magnetic resonance imaging (MRI) techniques, have been used to directly visualize blood flow through the brain, as demonstrated by nearly 5000 entries for [(MRI) AND (blood flow) AND (brain)] in PubMed (National Library of Medicine, Bethesda, MD, Pubmed (2010)). Although computed tomography (CT) or MRI are

routinely used for diagnosis or experiments (reviewed by Giachetti and Zanetti (2006)), the possibilities of using MRI and CT for quantitative description and quantification of vessel orientation are less obvious (Inoue, 2010; Schlageter et al., 1999). The quantification of vascular or blood flow parameters in various visualization techniques (imaging, histology, etc.) allows for statistical comparisons between different conditions, such as healthy and diseased brains, untreated and treated tissue or gray and white matter from different brain regions. However, if the goal is to link changes in circulation to certain pathological changes in the nervous tissue or if the resolution of the chosen imaging method is not sufficient for the topic of interest, histological examination of brain samples is still necessary (Grinberg et al., 2009; Kiselev et al., 2005). In addition, the orientation of vessels within the brain determines their visibility in different imaging techniques (Park et al., 2008). Quantitative data on vessel

\* Corresponding author. Tel.: +420 377632364; fax: +420 377632302.

E-mail addresses: [kochovap@kme.zcu.cz](mailto:kochovap@kme.zcu.cz) (P. Kochová), [cimrman3@ntc.zcu.cz](mailto:cimrman3@ntc.zcu.cz) (R. Cimrman), [janacek@biomed.cas.cz](mailto:janacek@biomed.cas.cz) (J. Janáček), [Kirsti.Witter@vetmeduni.ac.at](mailto:Kirsti.Witter@vetmeduni.ac.at) (K. Witter), [tonar@ntc.zcu.cz](mailto:tonar@ntc.zcu.cz), [Zbynek.Tonar@lfp.cuni.cz](mailto:Zbynek.Tonar@lfp.cuni.cz) (Z. Tonar).

orientation might provide important insight into changes in brain perfusion and thus neuronal function (Gardner, 2010) and represent a prerequisite for modeling cerebral blood flow.

### 1.1. Geometrical representation of blood vessels as oriented branching fibers

In biology, systems of oriented and branching lines or fibers are often used to represent the three-dimensional (3D) directionality and topology of microscopic blood vessels supplying various organs. The blood microvessels comprise arterioles, metarterioles, capillaries and venules. These objects can be quantified by their volume, surface area, length, cross-sectional area, vessel diameter, vessel number/microvessel density, tortuosity, intervessel distance and their spatial arrangement can be visualized (Schlageter et al., 1999; Park et al., 2008; Bullitt et al., 2009; Ding et al., 2008; Janáček et al., 2009; Jirkovská et al., 2002; Jirkovská et al., 2008; Konerding et al., 1995; Kubínová et al., 2001; Kubínová and Janáček, 2001; Lametschwandtner et al., 2004; Mathieu et al., 2006; Salu et al., 2002; Tonar et al., 2011).

References to the orientation of cerebral blood microvessels are usually made with respect to conventional anatomical planes and directions, e.g., antero-posterior, latero-lateral, radial, tangential, etc. However, if a statistical description of hundreds or thousands of microvessel orientations in each sample is required, tools for analyzing and summarizing these systems are necessary. For maximal data mining, such tools should also identify any preferential directions, if possible.

The two of the most frequently used characteristics that can be used to conceptually describe the fiber orientation are the rose of directions and the rose of intersections (Mecke, 1981; Rataj and Saxl, 1989). The rose of intersections (Fig. 1A) is a polar plot of the mean density of intersections of the fiber system with a line of given orientation (Spodarev, 2001; Spodarev, 2003; Stoyan et al., 1996; Sundararaghavan and Zabarar, 2004). Briefly, an image of the fiber system is intersected by lines in various directions and the number of intersects or the variation of gray level (in the case of gray scale digital images) along the lines is observed. The orientation distribution is related to the intensity of the intersections in relevant directions (Stoyan et al., 1996; Sundararaghavan and Zabarar, 2004).

The rose of directions (Fig. 1B) is defined as the length-weighted orientation of the segments, typically piecewise continuous curves (Stoyan et al., 1996; Tunak and Linka, 2007). The relationship between the rose of intersections and the rose of

directions has been described by several groups (Beneš and Gokhale, 2000; Kiderlen and Pfrang, 2005; Prokešová, 2003).

Both the rose of intersections and rose of directions allow for the numerical description of the orientation of each line segment (e.g., each vessel) in a system and their assignment to classes for further statistical analysis (Stoyan et al., 1996; Howard and Reed, 1998). Furthermore, these measures provide a first impression of the uniformity or non-uniformity of fiber (e.g., blood vessel) orientation, known as isotropy or anisotropy (see below). The degree of anisotropy of a cerebral vascular tree might represent an additional important measure that characterizes nervous tissue nutrition and function (cf. Inoue, 2010; Schlageter et al., 1999; Gardner, 2010).

### 1.2. Exploring of blood vessel orientation in the form of numerical data

In the two-dimensional (2D) evaluation of line systems, a plane can be divided into as many equiangular parts as the accuracy required with respect to the length density. Individual parts are characterized by angle intervals covering  $[0, 2\pi[$ . For example, the plane can be divided in 4 quadrants. In this case, one quadrant is given by angle interval  $[\langle k * (\pi/2), (k+1) * (\pi/2)[$ , where  $k=0, 1, 2, 3$ . The lengths of lines in individual regions are divided by the total length of all lines in the system to get the length density. These length densities are graphically represented by a polar plot (see Fig. 1B), giving information about the 2D anisotropy of system.

For numerical analysis of 3D line systems, such as cerebral blood vessels, the evaluation can essentially follow the 2D model. The space can be divided in regions given by angles of elevation (or latitude) and azimuth (or longitude) (Fig. 2E) in such a way that all tetragons on the surface of the sphere bounded by subsistent azimuths and elevations have equal area. Azimuths correspond to equiangular parts of the 2D case from the interval  $[0, 2\pi[$ . Elevations are from the interval  $[0, \pi/2[$  taking the symmetry with respect to the origin into account. The length densities of lines in given directions (regions) are counted and plotted into the rose of directions. If the spatial points of the rose of directions form a sphere, we can say that the system is isotropic.

### 1.3. Anisotropy and isotropy of line systems

Anisotropy is defined as a property of a system having a different value when measured in different directions. The an/isotropy of

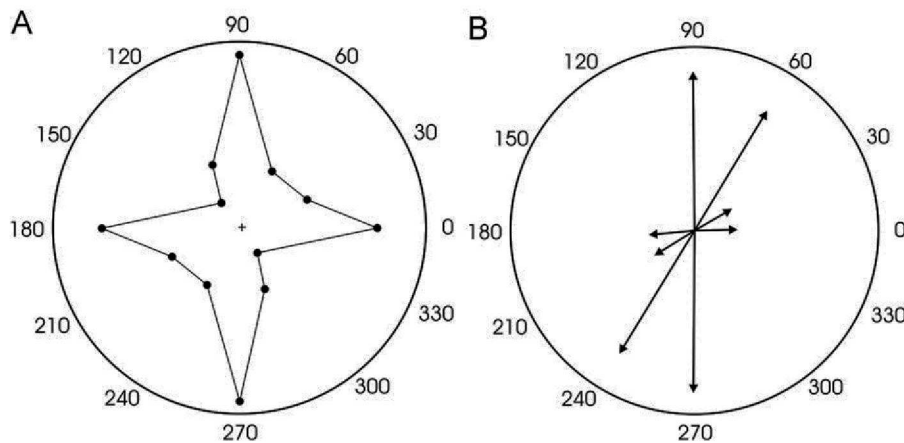


**Fig. 1.** (A) An illustration of the rose of intersection. The shape gives information about the an/isotropy of the structure. A circular shape means that the structure is isotropic, while the star-like spikes show the anisotropic arrangement of a system. (B) An illustration of the rose of directions. The arrows in individual directions show the length (or angular) density of the lines of a system in the associated direction. If there is a uniform distribution, the arrows have the same size. In the case of anisotropic system, the lengths of arrows are higher in the preferential directions. Angles are in degrees in both cases.

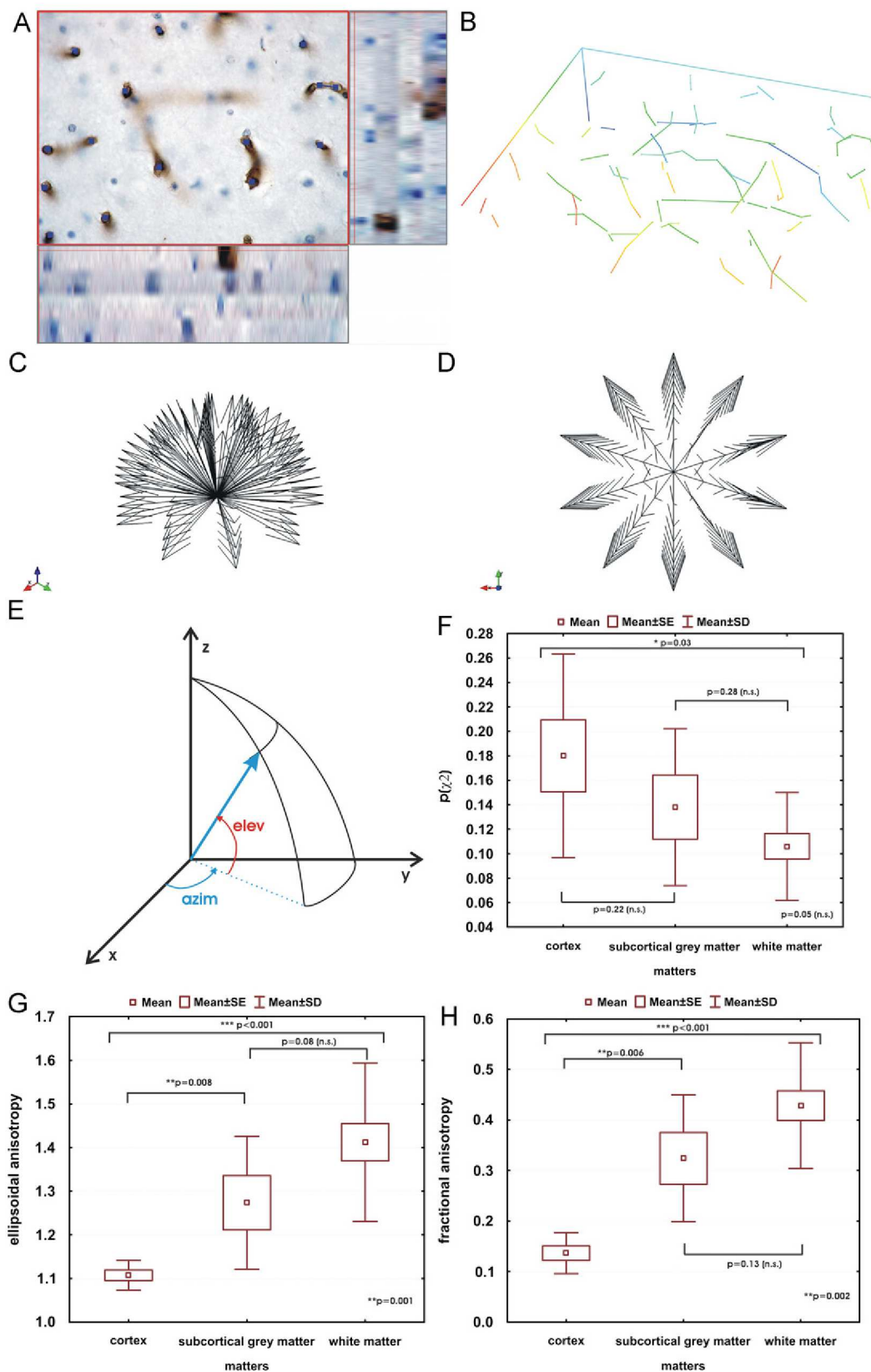


**Fig. 2.** (A) Tracing the microvessel profiles: the skeleton curves approximated by straight-line segments of all individual blood vessels and their branches. (B) System of oriented 3D lines representing the traced microvessels: the  $x$ -axis runs in the antero-posterior direction (to the right), the  $y$ -axis runs in the latero-lateral direction (to the front) and the  $z$ -axis runs in the supero-inferior direction (down) in relation to the human body (C, D). Upper hemisphere of the rose of directions corresponding to 10 parallels and 10 meridians, yielding 100 directions. The vectors head towards the middle of the tetragons bounded by individual parallels and meridians. The angle arrows show the directions of increasing values of parallels and meridians (starting in the zero). (C) Side view. (D) Upper view. The coordinate system in the left bottom corner corresponds to the coordinate system in (E). (E) The angular description of points on a sphere: azimuth or longitude (azim) and elevation or latitude (elev). Azimuths are from  $[0, 2\pi]$ , and elevations are from  $[0, \pi/2]$ . The frontal plane of the human body was defined by azimuths  $90^\circ$  ( $\pi/2$ ) and  $270^\circ$  ( $3\pi/2$ ). (F)–(H). The Kruskal–Wallis (right lower corner) and Mann–Whitney  $U$ -test for the  $p(\chi^2)$  (F), ellipsoidal (G) and fractional (H) anisotropy. The differences were significant when  $p < 0.05$  (\*); n.s. (not significant).

cerebral blood vessels could be described numerically as the non/uniformity of the spatial distribution of their length densities. For this purpose, the length density of vessels in a given direction is counted as the length of vessels in the given direction divided by the total length of all vessels in the brain, as described above. If the value of length density is uniformly distributed in all directions, we can claim the system to be isotropic. In the case of preferred directions with higher values of length density than in the other directions, the system is anisotropic. The level of anisotropy is given by the differences of length densities of lines in various directions. Small differences are connected with low levels of anisotropy, and the system is closer to being isotropic. Conversely, high differences are associated with high levels of anisotropy. In terms of a mathematical definition, these facts can be formulated as follows: if a stationary fiber process has a rotation-invariant distribution, it is considered to be isotropic, otherwise it is anisotropic Kiderlen and Pfrang (2005).

For statistical comparison, anisotropy has to be expressed as a mathematical value. Two standard methods have been described for this purpose: ellipsoidal and fractional anisotropy (Dryden et al., 2009). Both methods are based on counting eigenvalues of the length-weighted average tensor of the segment (vessels) orientation. For planar data, the current methodology provides a powerful tool for exploratory statistics in microscopy (Mattfeld, 2005), including the well-documented software *statstat* accessible to scientists for free (Baddeley and Turner, 2005). However, studies quantifying the spatial orientation of linear structures, such as cerebral microvessels, captured or reconstructed from serial physical or optical sections, are lacking. This led us to search for another method for quantifying orientation and make it available for other researchers investigating oriented microstructures.

#### 1.4. Aims of the study

We present a new method for evaluating an/isotropy using 2D physical and optical serial sections. The method is based on a 3D reconstruction of line systems built from the 2D sections using poly-line approximations and a  $\chi^2$ -test. Following the definition of isotropy given above, we suggest that if a stationary fiber process has a discrete uniform distribution, then it can be regarded as isotropic, while the observed distribution can be compared with the expected one using the  $\chi^2$ -test. An open source software for the 3D evaluation of anisotropy of linear structures shall be developed.

In detail, our aims were as follows:

- i) to evaluate the applicability of the  $p(\chi^2)$  method in a routine microscopic study and to determine the rose of directions of linear systems representing microscopic blood vessels in samples of human brains, thus presenting a new tool for scientists dealing with the isotropy and orientation of microscopic structures,
- ii) to use the length densities of blood vessels to determine the preferential directions covering 50% of blood vessel density in various regions of the brains, and this value was chosen *ad hoc*,
- iii) to compare the  $p(\chi^2)$  method based on the assumption of a discrete uniform distribution of length densities with two other methods used to determine anisotropy in 3D space, namely ellipsoidal and fractional anisotropy (Dryden et al., 2009).

## 2. Materials and methods

### 2.1. Specimen preparation

Samples of brain tissue were taken from inward patients, a healthy 53-year-old woman (brain 1) and a 70-year-old man with presumed vascular microscopic atrophy (brain 2), who died in the Department of Neurology, University Hospital in Pilsen. Both patients underwent pathological autopsy on request of the authorities of the Department. This autopsy was performed to confirm the clinical diagnoses and to evaluate the effects of the treatment according to the Acts No. 20/1996, 19/1988 valid in the Law of the Czech Republic. In both patients, the pathological autopsy revealed that the cause of death was not related to any obvious deterioration of brain tissue. As the Health Act and the Burial Act cited above explicitly permits to take tissue samples from the pathological autopsy for the purpose of medical research, the pathological anatomist saved the slabs of the brains for the purpose of our study. Sixteen tissue samples (approx.  $1 \times 1 \times 1 \text{ cm}^3$ ) were taken from the left hemisphere of each brain, representing the cerebral cortex, subcortical gray matter, white matter, pons and cerebellum (see Table 1). The anatomical localization of the tissue blocks was macroscopically verified according to Standring et al. (2008). The gray matter was discriminated microscopically based on the grouping of neuronal cell bodies, while the white matter was identified as an accumulation of axons, mostly ensheathed in pale colored myelin. Due to

**Table 1**  
Anatomical origin of individual tissue samples.

Brain region	Sample number		Matter
	Brain 1	Brain 2	
Cortex supplied by the anterior cerebral artery	HB1	HB14	Cortex
Cortex supplied by the middle cerebral artery	HB2	HB15	Cortex
Cortex supplied by the posterior cerebral artery	HB3	HB16	Cortex
Subcortical gray matter—the putamen	HB4	HB17	Subcortical gray matter
Subcortical gray matter—the globus pallidus	HB5	HB18	Subcortical gray matter
Subcortical gray matter—the thalamus	HB6	HB19	Subcortical gray matter
Subcortical white matter, anterior cerebral artery	HB7	HB20	White matter
Subcortical white matter, middle cerebral artery	HB8	HB21	White matter
Subcortical white matter, posterior cerebral artery	HB9	HB22	White matter
White matter, anterior/middle cerebral artery	HB10	HB23	White matter
White matter, middle/posterior cerebral artery	HB11	HB24	White matter
White matter, internal capsule, anterior limb	HB12	HB25	White matter
White matter, internal capsule, posterior limb	HB13	HB26	White matter
Pons, ventral part, pedunculus cerebri	HB27	HB30	White matter
Cerebellum white matter	HB28	HB31	White matter
Cerebellum cortex	HB29	HB32	Cortex

the counterstaining used for cell bodies (see below), the difference between the gray and white matter was clearly visible and unambiguous. Each of the 32 tissue samples was then divided into three smaller blocks with cutting planes oriented into frontal, sagittal and transversal directions. All tissue blocks ( $n=96$ ) were handled separately and their orientation was kept carefully during processing. The tissue samples were fixed in buffered formalin according to Lillie (Romeis, 1989) at room temperature for minimally one week. Afterwards, the samples were rinsed in 70% ethanol, dehydrated in increasing alcohol concentrations and routinely embedded in paraffin using a shandon excelsior tissue processor.

All tissue blocks were cut into series of four consecutive 20- $\mu\text{m}$  thick histological sections, referred to as slabs in stereological nomenclature. The slabs were mounted on Super Frost slides coated with (3-aminopropyl)triethoxysilane (Sigma-Aldrich, Vienna, Austria), deparaffinized, rehydrated and permeabilised with chilled acetone ( $-20^\circ\text{C}$ ) for 10 min. Afterwards, the sections were transferred to phosphate buffered saline (PBS, pH 7.4). Endogenous peroxidase activity was blocked with 0.6% (v/v)  $\text{H}_2\text{O}_2$  in distilled water by non-specific binding activity with normal goat serum (DakoCytomation, Glostrup, Denmark; 150  $\mu\text{l}$ /10 ml PBS) at room temperature. For antigen retrieval, the sections were digested with 1 mg protease from *Streptomyces griseus* (Sigma, Vienna, Austria)/ml PBS for 20 min at room temperature. All sections were incubated overnight with a polyclonal rabbit anti-rat laminin antibody (DakoCytomation, Glostrup, Denmark, 1:500) at  $4^\circ\text{C}$ . The immune reaction was detected using the anti-rabbit PowerVision Kit (Immunovision Technologies, Daly City, CA, USA) according to the manufacturer's instructions. The reaction was visualized with diaminobenzidine (Sigma-Aldrich, Vienna, Austria) in 0.03% (v/v)  $\text{H}_2\text{O}_2$  in TRIS-buffered saline (pH 7.4). All sections were counterstained with Mayer's hematoxylin, dehydrated and mounted with a medium soluble in xylene. From each slab, four stacks comprising three 6- $\mu\text{m}$  thick optical sections were taken in a systematic, uniform, random manner (48 micrographs per orientation and 144 micrographs per brain tissue sample). The optical sections were taken using an oil immersion objective ( $60\times$ , numerical aperture 1.35) mounted on the microscope Olympus BX51. Using a programmable motorized Z-stage, the thickness of all the sections was carefully measured in every field of vision to exclude any thick sections with a non-uniform deformation (i.e., sections with a conspicuous local variation in the deformation). Therefore the real height of all the stacks of three optical sections used for the study was uniform and was equal to 18  $\mu\text{m}$ . The shrinkage of tissue during histological processing has not been measured, since we did not expect an effect on vessel orientation. Although the paraffin embedding used in our study leads to inevitable deformation of the tissue and to the z-axis distortion problem (Dorph-Petersen et al., 2001), the shrinkage should not affect the results of this study. The reason is that the result for each tissue sample was based on three small blocks representing all three anatomical directions, i.e., even an anisotropic z-shrinkage of individual physical sections would affect all three directions in the same way.

A countable microvessel was defined as any profile of laminin-positive outline separated from adjacent microvessels or elements of the nervous tissue. The existence of clearly visible vessel lumen, the size of the vessel caliber and the presence of erythrocytes were not included in the criteria for defining a microvessel.

## 2.2. Line systems representing the topology of brain microvessels

The skeleton curve approximated by straight-line segments of all individual blood vessels and their branches in the slabs were marked (Fig. 2A) and approximated by a system of branched linear structures (Fig. 2B). A linear segment was delimited

either by a microvessel branching node or by the appearance/disappearance of the microvessel within the slice. The total number of counted linear segments was 12 150, whereas 3128 segments were counted in 18 tissue samples of white matter, 3860 in six tissue samples of subcortical gray matter and 5162 in eight tissue samples of cortex. Thus, the mean number of linear segments per tissue sample was 173 per white matter, 643 per gray matter and 645 per cortex.

The orientation of the blood vessels for all brain regions was related to the coordinate system defined by the xy transversal plane (the x-axis was the antero-posterior, y-axis was the latero-lateral direction in relation to the human body), while the z-axis was the superio-inferior direction perpendicular to the transversal cutting plane. The resulting line systems depicting the number and orientation of microvessels in the brain (see Fig. 2B) were defined by the directions of the individual lines and their lengths.

## 2.3. Rose of directions and orientation

The preferential directions of lines representing the topology of brain microvessels were calculated as follows. The line systems described above were transformed into histograms. A virtual sphere was constructed in 3D real space using the aforementioned coordinate system: x-axis—the antero-posterior direction, y-axis—the latero-lateral direction and z-axis—the inferio-superior direction in relation to the human body. The upper hemisphere of this sphere, with respect to the z-axis, was discretized by dividing (tessellating) it into ten parallels and ten meridians in such a way that all spherical tetragons framed by these parallels and meridians had equal areas (Fig. 2C and D). Thus, we obtained 100 possible directions. The line systems representing the microvessels of the brain were classified according to their respective meridians, parallels and lengths and charted into the tessellated hemisphere. The length densities, meaning lengths of the lines in individual directions given by the parallels and meridians, were counted using the formula:

$$l(\text{frac})_{ij} = \frac{l_{ij}}{\sum_{j=1}^n \sum_{i=1}^n l_{ij}}, \quad (1)$$

where  $l(\text{frac})_{ij}$  is the length density of lines in the given direction,  $l_{ij}$  is the length of lines in that direction,  $\sum_{j=1}^n \sum_{i=1}^n l_{ij}$  is the total length of all lines,  $i, j$  are the indices of meridians and parallels and  $n=10$  is the total number of parallels and meridians, yielding 100 individual directions.

The  $l(\text{frac})_{ij}$  values were sorted in descending order and cumulatively added together to determine the number  $n_{\max}(f=0.5)$  of directions with the highest values of length densities covering 50% ( $\sum_{ij}^{n_{\max}(f=0.5)} l(\text{frac})_{ij} \geq 0.5$ ) of the total length. This value represents half of all blood vessels in the evaluated region and was chosen *ad hoc*. The obtained directions were labeled as the preferential directions of lines, representing the topology of the blood microvessels.

The greater the number of directions needed to cover 50% of the total length of microvessels, the more isotropic their orientation.

## 2.4. Discrete uniform distribution $p(\chi^2)$ method

To determine the isotropy of blood vessels in individual brain specimens, we used the Pearson's  $\chi^2$ -test. This test is based on a comparison between the distribution of the test statistics and the  $\chi^2$  distribution. In our case we calculated the  $\chi^2$  by

$$\chi^2 = \sum_{i=1}^N \frac{(o_i - e_i)^2}{e_i}, \quad (2)$$

where  $o_i$  represents the observed values (length density of blood vessels in individual directions),  $e_i$  represents the expected values and  $N$  is the number of cases (directions). In our study  $e_i$  corresponded to the discrete uniform distribution, i.e., values in the general population would occur in each cell (direction) with equal frequency:

$$e_i = 1/N, \quad (3)$$

where 1 is the total sum of the length densities of all directions and  $N=100$  is the total number of directions. Thus,

$$e_i = 1/100 = 0.01, \quad (4)$$

meaning

$$\chi^2 = \sum_{i=1}^N \frac{(o_i - 0.01)^2}{0.01}. \quad (5)$$

The  $\chi^2$  of the blood vessels was counted, and the corresponding probability density function  $p(\chi^2)$  was determined.

With these data we tested the following null hypothesis: the system of blood vessels is isotropic, meaning that the distribution of our results is equal to the discrete uniform distribution. The hypothesis should be rejected in the case of  $p(\chi^2) < 0.05$ .

### 2.5. Ellipsoidal and fractional anisotropy

To compare the anisotropy determined by the new  $p(\chi^2)$  method, we also computed the anisotropy by standard methods: ellipsoidal and fractional anisotropy, as described by Dryden et al. (2009). For each line segment of the traced capillaries  $\langle a, b \rangle$  with length  $L$  and with direction  $\underline{v} = (b - a)/L$ , we calculated the matrix  $\underline{v} \otimes \underline{v}^T = \{v_i \cdot v_j\}$ . Then we calculated the average matrix of all the segments  $T = \{t_{ij}\}$  weighted by length:  $T = \sum_k L_k \underline{v}_k \otimes \underline{v}_k^T$ , where the sum is over all line segments.

The ellipsoidal anisotropy and the fractional anisotropy were calculated from the eigenvalues of the average matrix  $T$ :  $\lambda_3 \geq \lambda_2 \geq \lambda_1 \geq 0$ , which can be calculated by the Jacobi algorithm (Press et al., 1992). The square roots of the eigenvalues correspond to the lengths of principal axes of the ellipsoid generated by the matrix  $T$  (Dryden et al., 2009).

Ellipsoidal anisotropy is calculated as a ratio of the length of the longest axis of the ellipsoid to the average of the lengths of the other two axes:

$$EA = 2\sqrt{\lambda_3} / (\sqrt{\lambda_1} + \sqrt{\lambda_2}), \quad (6)$$

where EA is ellipsoidal anisotropy and  $\lambda_i$ ,  $i=1, 2, 3$  are the eigenvalues of the average matrix  $T$ . The range of obtained numbers can span from 1 (isotropy: capillaries express no preferential direction) to infinity (total anisotropy: all capillaries run in the same direction).

Fractional anisotropy is calculated using Eq. (7), as described in the study by Dryden et al. (2009):

$$FA = \left( \frac{3}{2} \sum_{i=1}^3 (\lambda_i - \bar{\lambda})^2 / \sum_{i=1}^3 \lambda_i^2 \right)^{1/2}, \quad (7)$$

where FA is the fractional anisotropy,  $\lambda_i$ ,  $i=1, 2, 3$  are eigenvalues of the average matrix  $T$  and  $\bar{\lambda}$  is the mean value of the eigenvalues. The range of obtained numbers can span from 0 (isotropy) to 1 (total anisotropy).

All these computations, as well as the histogram evaluation, were done using our own open source software, esofspy, written in the Python programming language (version 2.6.5) (Python, 2001).

### 2.6. Statistics

The normality of  $p(\chi^2)$ , fractional and ellipsoidal anisotropy, and the number of directions ( $n_{max}(f=0.5)$ ) relevant to 50% of the length densities of all lines were tested using Shapiro–Wilk's  $W$ -test. The correlation between  $p(\chi^2)$ , fractional and ellipsoidal anisotropy and  $n_{max}(f=0.5)$  was evaluated with the Spearman correlation coefficient.

All of the following calculations were made separately for  $p(\chi^2)$ , fractional anisotropy and ellipsoidal anisotropy. The Wilcoxon matched pairs test was used to compare the anisotropy between the two brains. Samples of the same anatomical region from brain 1 and brain 2 were regarded as a pair. The Kruskal–Wallis test was used to test the differences between the different brain tissues (cortex, subcortical gray matter, white matter). The Mann–Whitney  $U$ -test was used to test the differences between two types of cerebral matters, such as cortex vs. subcortical gray matter, cortex vs. white matter and subcortical gray matter vs. white matter. The names and individual tissue types are given in Table 1.

## 3. Results

The Shapiro–Wilk's  $W$ -test showed that the  $p(\chi^2)$ , fractional anisotropy, ellipsoidal anisotropy and the  $n_{max}(f=0.5)$  did not have normal distributions.

### 3.1. Differences between the corresponding parts of the two brains

The values of  $p(\chi^2)$ , ellipsoidal anisotropy and fractional anisotropy are shown in Table 2. The Wilcoxon matched pair test did not show any significant differences in the levels of  $p(\chi^2)$  ( $p=0.92$ ), fractional ( $p=0.12$ ) and ellipsoidal anisotropy ( $p=0.09$ ) when corresponding regions from brain 1 and brain 2 were compared. Thus, for the purpose of further analysis, it was possible to process the values from both brains together.

### 3.2. Differences between the brain compartments

No significant differences in vascular an/isotropy were found between cortex, subcortical gray matter and white matter when comparing the values of  $p(\chi^2)$  using the Kruskal–Wallis test, but the value was very close to the boundary of significance ( $p=0.05$ ). Conversely, significant differences were found between cortex, subcortical gray matter and white matter when comparing the values of ellipsoidal ( $p=0.001$ ) and fractional ( $p=0.002$ ) anisotropy using the Kruskal–Wallis test.

In addition, there were no significant differences between cortex and subcortical gray matter ( $p=0.22$ ) and no significant difference between white matter and subcortical gray matter ( $p=0.28$ ) when the  $p(\chi^2)$  values were compared using the Mann–Whitney  $U$ -test (Fig. 2F). In contrast, a significant difference was discovered between white matter and the cortex ( $p=0.03$ ).

Similarly, there were no significant differences in vascular an/isotropy between subcortical gray matter and white matter in the case of ellipsoidal anisotropy ( $p=0.08$ ) or fractional anisotropy ( $p=0.13$ ) when the values of anisotropy were compared using the Mann–Whitney  $U$ -test (see Fig. 2G and H).

In contrast to the evaluation using  $p(\chi^2)$ , ellipsoidal anisotropy ( $p=0.008$ ) and fractional anisotropy ( $p=0.006$ ) indicated significant differences in anisotropy when comparing cortex and subcortical gray matter (Fig. 2G and H). Ellipsoidal and fractional anisotropy also found differences between cortex and white matter ( $p < 0.001$  in both cases).



**Table 2**

Values of an/isotropy for different samples of brain 1 and brain 2. Values of  $\chi^2$  and the corresponding values of  $p(\chi^2)$ , EA is the ellipsoidal anisotropy given by Eq. (6), FA is the fractional anisotropy given by Eq. (7) and the number of preferential directions covering 50% of the length density  $n_{max}(f=0.5)$ .

Brain 1	$\chi^2$	$p(\chi^2)$	EA	FA	$n_{max}$	Brain 2	$\chi^2$	$p(\chi^2)$	EA	FA	$n_{max}$
HB1	0.95	0.25	1.11	0.13	20	HB14	1.83	0.12	1.09	0.14	13
HB2	0.85	0.28	1.08	0.09	22	HB15	1.64	0.14	1.18	0.20	14
HB3	0.82	0.29	1.08	0.09	20	HB16	1.58	0.14	1.08	0.10	15
HB4	1.00	0.24	1.37	0.40	19	HB17	2.02	0.10	1.15	0.16	13
HB5	1.86	0.12	1.24	0.36	13	HB18	1.66	0.14	1.18	0.25	15
HB6	2.86	0.06	1.54	0.52	10	HB19	1.33	0.18	1.18	0.25	15
HB7	2.86	0.06	1.54	0.52	11	HB20	1.57	0.14	1.71	0.59	15
HB8	2.81	0.06	1.21	0.29	10	HB21	1.69	0.13	1.40	0.48	14
HB9	1.84	0.12	1.48	0.50	13	HB22	1.92	0.11	1.42	0.48	13
HB10	1.53	0.15	1.40	0.45	15	HB23	1.25	0.19	1.26	0.30	16
HB11	2.33	0.08	1.42	0.48	13	HB24	2.16	0.09	1.34	0.35	15
HB12	1.92	0.11	1.88	0.67	13	HB25	1.20	0.20	1.30	0.31	18
HB13	2.97	0.05	1.59	0.55	11	HB26	3.00	0.05	1.34	0.38	10
HB27	2.51	0.07	1.24	0.36	11	HB30	2.05	0.10	1.13	0.15	12
HB28	1.97	0.11	1.35	0.41	14	HB31	2.29	0.08	1.41	0.45	11
HB29	2.52	0.07	1.12	0.15	10	HB32	1.60	0.14	1.12	0.18	15

**Table 3**

Significant differences between the levels of anisotropy using  $p(\chi^2)$  values and values of ellipsoidal (EA) and fractional (FA) anisotropy for comparison; yes—significant differences; no—no significant differences.

Compared values	$p(\chi^2)$	EA	FA
Brain 1 vs. brain 2	No	No	No
Cortex vs. subcortical gray matter vs. white matter	No (limit)	Yes	Yes
Cortex vs. subcortical gray matter	No	Yes	Yes
Subcortical gray matter vs. white matter	No	No	No
Cortex vs. white matter	Yes	Yes	Yes

The significant differences found between the levels of anisotropy using  $p(\chi^2)$  values and values of ellipsoidal and fractional anisotropy are summarized in Table 3.

### 3.3. Assessment of the orientation of microvessels in the brain

The distribution of lengths of blood vessels per orientation (intervals of meridians and parallels) was computed and plotted as 2D plots of length densities for all specimens (examples are given in Fig. 3A and B). Similarly, the distribution of length densities determined by Eq. (1) were also evaluated (Fig. 3C and D). Furthermore, the Lambert azimuthal equal-area projection was used for the polar plots of the preferential directions (Fig. 3E and F).

### 3.4. Correlation between the anisotropy of cerebral microvessels and their preferential directions

The correlation between the values of  $p(\chi^2)$ , fractional anisotropy, ellipsoidal anisotropy and the number of preferential directions ( $n_{max}(f=0.5)$ ) is shown in Table 4. A high positive correlation between  $p(\chi^2)$  values and the  $n_{max}(f=0.5)$  was found (Spearman  $R=0.91$  and  $0.78$  for brain 1 and 2, respectively). Thus, a higher level of isotropy ( $p(\chi^2)$ ) was connected with a higher number of preferential directions.

A medium negative correlation was obtained between ellipsoidal and fractional anisotropy and the number of preferential directions ( $n_{max}(f=0.5)$ ). The ellipsoidal anisotropy was highly correlated with fractional anisotropy, and both were negatively correlated with  $p(\chi^2)$ .

### 3.5. Software

For to evaluate the spatial orientation of fiber systems, the program esofspy (evaluation of spatial orientation of fiber

systems in Python) written in the Python programming language (version 2.6.5) (Python, 2001) was developed. It allows for the automatic postprocessing of 2D plots of length densities and roses of directions, as well as the evaluation of preferential directions and the an/isotropy of line systems. The basic functions cover the following:

- reading and loading of input data (text file with three columns: number of meridians, number of parallels, length of lines associated with one pair of a meridian and a parallel),
- construction of roses of directions,
- assessment of preferential directions based on a threshold (e.g., 50% of the total length of lines) or on a given number of directions,
- vectors of preferential directions,
- evaluation of an/isotropy based on the  $\chi^2$ -test, ellipsoidal and fractional anisotropy,
- graphical interpretation of results (2D plots of lengths of lines, 2D plots of length densities of lines, roses of directions),
- saving of results.

We employed standard program packages, such as numpy (version 1.3.0), matplotlib (version 0.99.1) and ipython (version 0.10). This software is applicable to various types of line systems and is open source software that can be found and downloaded at Gensei (2010). The esofspy is supplemented by documentation and an example.

## 4. Discussion

In general, the assumption that vessel orientation in the human brain does not differ between regions and between white and gray matter (Schlageter et al., 1999), could not be verified in this work. Both orientation and an/isotropy were different in the different parts of the analyzed brains in this study. Roses of orientation and 2D plots of the length densities were both suitable for visualizing the orientation and distribution of the cerebral microvessels. The novel  $\chi^2$ -test and the ellipsoidal and fractional anisotropy values showed differences in anisotropy between the studied brain regions equally well.

### 4.1. Graphical presentation of blood vessel orientation

The majority of blood vessels in the human brains investigated for our study were oriented in the plane of azimuth  $90^\circ$  and  $270^\circ$ ,

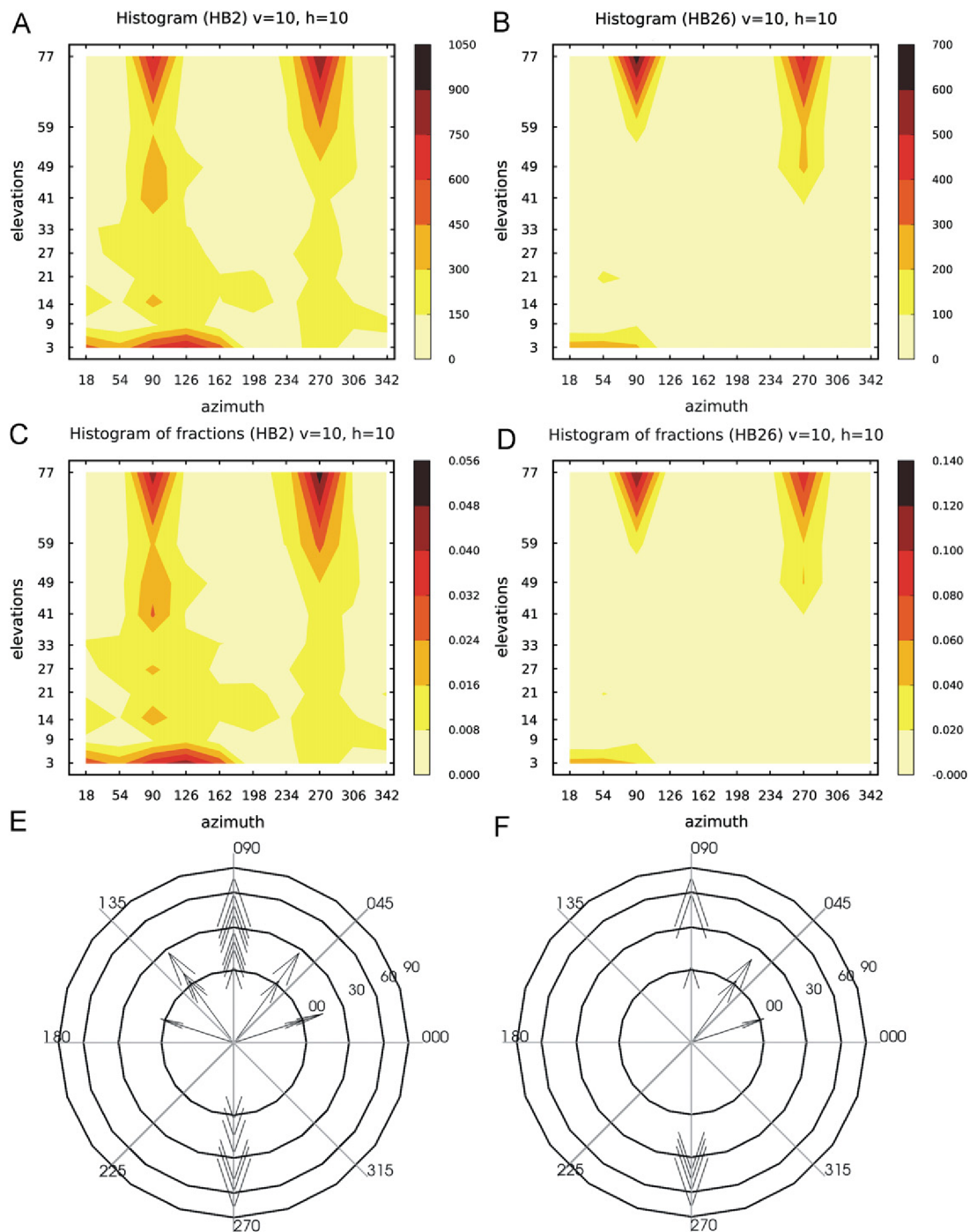


**Fig. 3.** (A, B) Examples of the 2D plot plots of the lengths of blood vessels in given directions: HB2 ((A) anisotropic) and HB26 ((B) anisotropic with preferential directions). The color scale corresponds to the lengths (dark regions represent a high value of length of the microvessels in a given direction),  $v$  is the number of parallels and  $h$  is the number of meridians (corresponding to Fig. 2C and D). (C, D) Examples of 2D plots of the length densities of blood vessels given by Eq. (1): HB2 ((C) anisotropic) and HB26 ((D) anisotropic with preferential directions). The color scale corresponds to length densities (dark regions represent a high value of length density of the microvessels in a given direction),  $v$  is the number of parallels and  $h$  is the number of meridians (corresponding to Fig. 2C and D). (E, F) Examples of the direction of blood vessels covering 50% of the length of all blood vessels in the brain specimen: HB2 ((E) isotropic system with many preferential directions, namely 22,  $p(\chi^2)=0.28$ ) and HB26 ((F) isotropic system with a few preferential directions, namely 10, near the boundary of significance  $p(\chi^2)=0.05$ ). The Lambert azimuthal equal-area projection was used for the polar plots. Radial lines are azimuths, concentric circles are elevations. The arrows indicate individual directions. (For interpretation of the references to color in this figure legend, the reader is referred to the web version of this article.)

i.e., the frontal plane. This is shown by a rose of directions or even better by 2D plots of length density and preferential directions of all specimens (examples are shown in Fig. 2A–D). In contrast to the uniform distribution of azimuths, the variability in the value of elevation visible on preferential directions and the 2D plots of length density was smaller in the subcortical gray matter, pons

and cerebellum than in the cortex of brain 1. That is to say, in the cortex, vessels run in all possible directions, whereas in the subcortical gray matter, pons and cerebellum, certain elevations are preferred. This was not observed in the case of brain 2. The explanation of these differences between the brains is unclear. The microvascular atrophy of brain 2, the different gender of the

**Table 4**

Spearman rank order correlations between the quantitative parameters describing an/isotropy of cerebral microvessels for both brains together:  $p(\chi^2)$  stands for the probability density function,  $n_{max}(f=0.5)$  stands for the numbers of preferential directions, EA stands for ellipsoidal anisotropy and FA stands for fractional anisotropy. All correlations are significant at  $p < 0.05$ .

	$p(\chi^2)$	$n_{max}(f=0.5)$	EA	FA
$p(\chi^2)$	–	0.91	–0.42	–0.42
$n_{max}(f=0.5)$	–	–	–0.39	–0.41
EA	–	–	–	0.99
FA	–	–	–	–

donors or the different ages of the donors could all be involved, but the influence of these factors on vessel orientation has not yet been published.

There are only very few studies dealing with the quantification of blood vessel orientation in the brain. Cassot et al. (2006) concentrated on a novel 3D computer-assisted method for a quantitative study of the microvascular networks of the collateral sulcus in the temporal lobe. The 2D evaluation was used with division into 24 intervals of  $7.5^\circ$ , and the frequency distribution was plotted. To classify the orientation heterogeneity, the interquartile range of this frequency distribution was determined. A small range is indicative of a more uniform vessel orientation, while a larger range suggested a more heterogeneous vessel orientation.

Only a few other methods have been described for the visualization of blood vessel orientation in other organs, such as the liver, muscles, placenta, intestinal wall and the wall of large blood vessels (Janáček et al., 2009; Jirkovská et al., 2002; Jirkovská et al., 2008; Lametschwandtner et al., 2004; Čebašek et al., 2010; Gutkowski et al., 2004; Kachlik et al., 2010; Lametschwandtner et al., 2005; Mathieu et al., 1983; Mayhew and Jairam 2000; Rieder et al., 1995). Most of them are based on 3D approaches. Rieder et al. (1995) presented a computerized method for determining microvascular in rat muscles. The 2D rose plot of vessel density estimated at different grid orientations using  $5^\circ$  increments showed a random orientation of blood vessels. Gutkowski et al. (2004) described an algorithm for the directional analysis of digitalized 3D images by configuration counts. The authors extended the 2D version (Kiderlen and Jensen, 2003) of a method for estimating the oriented rose of binary planar images using voxel cubes. Mathieu et al. (1983) used the Fischer distribution model of the rose of directions to determine the degree of anisotropy of capillaries in skeletal muscle tissue. Some of these methods assume 3D input data (voxel) and cannot be used in the case of our physical and optical sections. Others are equivalent to our quantification, but have to be supported by a complex mathematical apparatus. This was one of the reasons why we used the  $p(\chi^2)$  method for the quantification of brain microvessels. Moreover, these methods are not fully accessible as an open source code.

Another reason for using the  $p(\chi^2)$  method is that the  $\chi^2$  analysis is already an acknowledged method used in stereology, e.g., as the relative labeling index (Mayhew et al., 2002; Mayhew et al., 2009). There is a lot of experience with this method among the biologist who are usually familiar with using and interpreting it whenever testing differences between observed and random distributions.

#### 4.2. The $p(\chi^2)$ method—numerical assessment of the orientation of cerebral blood vessels

As described above, some 2D plots of length density showed a high concentration of blood vessels in a few directions for certain parts of the human brain (Fig. 3B and D), whereas other 2D plots demonstrated a diffusion of blood vessels into more directions (Fig. 3A and C). The level of an/isotropy determined by the  $\chi^2$ -test

corresponded with this graphical presentation. However, the values of  $p(\chi^2)$  ranged from 0.05 and 0.30 and were not sufficient to contradict the null hypothesis that the system of blood vessels was isotropic. It seems that a classification of anisotropy based on the widely used threshold of  $p < 0.05$  was not very helpful when applied to our results.

##### 4.2.1. Choice of level of significance for the $p(\chi^2)$ method

Choosing a level of significance is an arbitrary task. The conventional level of 5% was chosen initially when evaluating our newly introduced  $p(\chi^2)$  method. However, statistical significance and biological importance are not necessarily equivalent, as shown in the studies by Altman and Bland (1995). Our results suggest that the conventional 5% level can be best used if extreme conditions are to be described. However, this condition would occur only rarely in biological systems.

In case of entirely isotropic system (according to a discrete uniform distribution) we get a value close to  $p(\chi^2)=1$ , while in the case of a system with few main directions, we get values lower than 0.001. Although our analyses did not yield such clear results, we can declare the system of human cerebral microvessels studied to be anisotropic, because the number of directions covering 50% of the total length of blood vessels (preferential directions) was lower than 22 (out of 100) in all cases. This can be regarded as a biologically important finding from the morphological and functional point of view.

If we used the conventional criterion “significant at  $p < 0.05$ ” for blood vessel orientation in the human brain, all regions would be defined as isotropic, even though the  $p$ -value was close to 0.05 in some cases. The level of anisotropy might be continuous with values changing slowly between individual regions. These changes could depend on several factors, including the presence or absence of large blood vessels in the neighboring area of individual regions. As long as information regarding the real biological significance of the formally assessed an/isotropy remains scarce, the 5% threshold still holds as a matter of convention, until more empirical data is collected and related to the functional characteristics of blood vessels, such as the quality of perfusion of the tissue, proneness to hypoxia, etc.

##### 4.2.2. Regional and inter-individual differences of blood vessel anisotropy in the human brain assessed by the $p(\chi^2)$ method

Microvessels in the white matter were, in general, more anisotropic than those in the cortex (see Fig. 2F and Table 2). This result is in agreement with the fact that the microvascular bed in the white matter is spatially arranged in parallel to the processes of neurons and neuroglial cells (Inoue, 2010). On the other hand, the blood vessels in the cortex were arranged more “randomly”, i.e., more isotropically. The subcortical gray matter represented an intermediate state.

For modeling purposes, the microvascular bed in the cortex should therefore be considered an isotropic network, while the microvessels supplying the white matter should be modeled as an anisotropic and direction-sensitive system. This also gave us foundation to evaluate the preferential directions ( $n_{max}(f=0.5)$ ), namely the directions covering 50% of total length of microvessels.

#### 4.3. Correlation between methods of mathematical anisotropy detection

##### 4.3.1. Ellipsoidal and fractional anisotropy in comparison with the $p(\chi^2)$ method

In general, ellipsoidal and fractional anisotropy provided similar results as the novel  $p(\chi^2)$  method (Table 3). The main difference between the methods was that ellipsoidal and fractional anisotropy

1 detected significant differences between the cortex and subcortical  
2 gray matter, whereas  $p(\chi^2)$  did not.

3 We processed the same data with all three methods to  
4 compare the results of ellipsoidal and fractional anisotropy  
5 against the  $p(\chi^2)$  method. While the ellipsoidal and fractional  
6 anisotropy yielded lower variability for the isotropic cortical  
7 microvessels, the variability of these methods increased substan-  
8 tially for the more anisotropic microvessels supplying the white  
9 matter (according to the mean  $\pm$  SD plotted in Fig. 2G and H).  
10 Conversely, the  $p(\chi^2)$  method had a higher variability in isotropic  
11 cortical vessels and a lower variability in anisotropic white matter  
12 vessels (Fig. 2F). This reflects different sensitivities to different  
13 levels of an/isotropy and also explains why the  $p$ -level was higher  
14 in the  $p(\chi^2)$  method (Fig. 2F) than in the ellipsoidal and fractional  
15 anisotropy methods (Fig. 2G and H) when testing the difference  
16 between the subcortical gray and the white matter. For exactly  
17 the same reason, the  $p(\chi^2)$  method considered the differences  
18 between the cortex and subcortical gray matter to be non-  
19 significant (Fig. 2F), while the ellipsoidal and fractional anisotropy  
20 were able to detect this difference (Fig. 2G and H) due to the  
21 lower variability of the compared data sets. Therefore, we suggest  
22 that ellipsoidal and fractional anisotropy are more sensitive for  
23 comparing isotropic vs. anisotropic structures and when analyz-  
24 ing the variability among several anisotropic structures (such as  
25 microvessels in various samples of white matter). Isotropic  
26 structures yielded very similar results in these two methods.  
27 When mutually comparing several isotropic structures (such as  
28 several samples of gray matter), the  $p(\chi^2)$  method would be more  
29 useful, as it is more sensitive within the range of isotropic  
30 samples.

#### 33 4.3.2. Correlation between anisotropy and preferential directions

34 The high linear dependence between  $p(\chi^2)$  and the number of  
35 preferential directions ( $R=0.91$ ) is related to the fact that both  
36 quantities are computed using the same methodology based on  
37 the length densities of lines of a system. Brain regions with an  
38 isotropic microvascular bed, and therefore a high value of  $p(\chi^2)$ ,  
39 also had more preferential directions covering 50% of all length  
40 densities in comparison with other brain regions with an aniso-  
41 tropic system of blood vessels, where only a few preferential  
42 directions could be detected.

43 This finding was furthermore validated by the fact that the  
44 brain specimens with a  $p(\chi^2)$  value around 0.06, i.e., regions with  
45 a less isotropic microvascular bed, such as white matter, had at  
46 least one value of length density fraction (one direction) higher  
47 than 10%. On the other hand, the samples with isotropic capillary  
48 orientation and a  $p(\chi^2)$  value around 0.25 (e.g., cortex) had a  
49 uniform distribution of length densities with only about 3% in any  
50 preferential direction.

51 The high level of correlation shows that the  $p(\chi^2)$  method  
52 based on comparison with the discrete uniform distribution used  
53 for the evaluation of anisotropy of a linear system has high  
54 potential for the determination of the number of preferential  
55 directions in line systems. The number of preferential directions  
56 is useful, especially for computational models that include the  
57 anisotropy and orientation of fibers (Cimrman and Rohan, 2010;  
58 Holzapfel and Gasser, 2001; Kochová et al., 2009).

59 The values determined by ellipsoidal and fractional anisotropy  
60 are based on the same methodology, and this connection gives  
61 them a high level of linear dependency with a factor of 0.99.  
62 However, the relationship between these anisotropies and the  
63 number of preferential directions is less considerable than in the  
64  $p(\chi^2)$  method. The negative linear correlation with preferential  
65 directions is, in both cases, about  $-0.4$ . When comparing the  
66 anisotropy of cortex, subcortical gray matter and white matter of

67 the brain, ellipsoidal and fractional anisotropy are more sensitive  
68 with respect to the determination of the differences in anisotropy  
69 between individual parts.

#### 71 4.4. Applicability of anisotropy detection for further linear 72 biological systems

73 The use of geometrical representations of fibers and branched  
74 line systems is not limited to vascular research only. A wide-  
75 spread range of fields could benefit from the approaches pre-  
76 sented in this paper. In biology, fiber systems are analyzed in  
77 research on cell proliferation (Boehm et al., 2010; Pruynne and  
78 Bretscher, 2000), morphogenesis of organs (Ranucci et al., 2000),  
79 models of villi and intervillous pores in placentas (Mayhew and  
80 Jairam, 2000), arrangement of cellulose microfibrils in plants  
81 (Aouar et al., 2010; Dumais et al., 2006; Emons and Mulder,  
82 1998; Geitmann and Ortega, 2009) and the organization of  
83 collagen fibers within the blood vessel wall (Holzapfel, 2006). In  
84 general, fibrillar structures of the cytoskeleton or extracellular  
85 matrix, as well as tubular structures (vessels, ducts etc.) and the  
86 fiber-like structures of certain cells (e.g., axons and dendrites of  
87 neurons), can be described mathematically in terms of their  
88 orientation and anisotropy.

89 Investigating the structural properties of biological tissues is  
90 often motivated by their biomechanical properties. These are  
91 known to be affected by fiber density, geometry, architecture  
92 and orientation (Holzapfel, 2006). However, the relationship  
93 between the structural and mechanical anisotropy of a tissue is  
94 not always straightforward. Some tissues have both isotropic and  
95 anisotropic components, such as dentine, in which the structural  
96 anisotropy of collagen fibrils is balanced with the anisotropy of  
97 overall crystal orientation (Guan et al., 2006).

98 Information on mathematical quantities describing fiber sys-  
99 tems helps us to understand the behavior of these fiber systems,  
100 and thus, can be applied in the computational modeling of  
101 systems to predict various situations that can occur in real  
102 processes and are hard to obtain (Tonar et al., 2011; Cimrman  
103 and Rohan, 2010; Holzapfel and Gasser, 2001; Kochová et al.,  
104 2009; Dumais et al., 2006; Geitmann and Ortega, 2009; Holzapfel,  
105 2006). The manufacturing of bionic and other materials copying  
106 organic systems (e.g., Mathieu et al., 2006; Dado and Levenberg,  
107 2009; Hou et al., 2003; Hutmacher, 2000; Kim et al., 2006;  
108 Lim and Donahue, 2007) will also require this information. Thus,  
109 materials with optimal properties can be fabricated, e.g., papers,  
110 insulators, or furniture elements (Lux et al., 2006). Moreover, the  
111 3D analysis of spatial arrangement, spatial orientation and  
112 preferential directions of fiber-like structures is a frequent  
113 problem in many scientific branches, including metallography  
114 (Wejrzanowski et al., 2008), the textile industry (Tunak and Linka,  
115 2007), topology of surface textures (Josso et al., 2005), plant  
116 biology (Aouar et al., 2010; Emons and Mulder, 1998; Geitmann  
117 and Ortega, 2009; Guan et al., 2006; Lhotáková et al., 2008) and  
118 tissue modeling (Tonar et al., 2011; Holzapfel and Gasser, 2001;  
119 Kochová et al., 2009; Dumais et al., 2006; Holzapfel, 2006) and  
120 still represents a challenge for the mathematical community  
121 (Tonar et al., 2011).

## 122 5. Conclusion

123 Based on the example of the blood microvessels in the human  
124 brain, we presented a novel method that can be used to obtain the  
125 rose of directions and to evaluate the anisotropy of a branching  
126 line system using a 3D reconstruction from physical and optical  
127 2D sections. This  $p(\chi^2)$  method is based on the comparison of the  
128 line system under study with a discrete uniform distribution and

was implemented into an open source software (Gensei, 2010) using the Python programming language.

The roses of directions and the anisotropy of blood vessels in various regions of two human brains were determined. Furthermore, the length densities were assessed and used to determine the orientation (vectors of azimuths and elevations) and the number of preferential directions covering 50% of total length of blood vessels in various regions of the brains. The results showed different levels of anisotropy for blood vessels in the human brain. The anisotropy and preferential orientation of blood vessels might differ between men and women or be influenced by age or disease. However, the main orientation of vessels in the white matter in the frontal plane was preserved for our two specimens.

Our  $p(\chi^2)$  method does not comply with the simple determination of significance by  $p=0.05$  criterion, but it can be used to determine differences between various parts of the studied materials, as demonstrated for the white matter and cortex of the human brain. The advantage of the  $p(\chi^2)$  method is its high correlation with the number of preferential directions of the line system. In contrast, ellipsoidal and fractional anisotropy seemed more sensitive for determining the differences of anisotropy between individual parts.

The  $p(\chi^2)$  method, as well as ellipsoidal and fractional anisotropy, can be calculated and compared using our platform-independent open source software esofspy, thus making the methods freely available to the scientific community.

## Q1 Uncited reference

Kärkkäinen and Jensen (2001).

## Acknowledgments

The development of the quantification techniques was supported by the ~~Grant Agency of the Czech Republic, Projects nos. 106/09/0740 and 109/09/P226~~. This work was also supported by the European Regional Development Fund (ERDF), project "NTIS—New Technologies for Information Society", European Center of Excellence, CZ.1.05/1.1.00/02.0090 and by the Academy of Sciences of the Czech Republic under Project no. AVOZ 50110509.

## References

- Altman, D.A., Bland, J.M., 1995. Statistics ~~notes—absence~~ of evidence is not evidence of absence. *BMJ* 311, 485.
- Aouar, L., Chebli, Y., Geitmann, A., 2010. Morphogenesis of complex plant cell shape: the mechanical role of crystalline cellulose in growing pollen tubes. *Sex. Plant Reprod.* 23, 15–27.
- Bullitt, E., Rahman, F.N., Smith, J.K., Kim, E., Zeng, D., Katz, L.M., Marks, B.L., 2009. The effect of exercise on the cerebral vasculature of healthy aged subjects as visualized by MR angiography. *AJNR* 30, 1857–1863.
- Beneš, V., Gokhale, A.M., 2000. Planar anisotropy revisited. *Kybernetika* 36, 149–164.
- Baddeley, A., Turner, R., 2005. Spatstat: an R package for analyzing spatial point patterns. *JSS* 12, 1–42.
- Boehm, B., Westerberg, H., Lesnicar-Pucko, G., Raja, S., Rautschka, M., Cotterell, J., Swoger, J., Sharpe, J., 2010. The role of spatially controlled cell proliferation in limb bud morphogenesis. *PLoS Biol.* 8, e1000420.
- Cassot, F., Lauwers, F., Fouard, C., Prohaska, S., Lauwers-Cances, V., 2006. A novel three-dimensional computer-assisted method for a quantitative study of microvascular networks of the human cerebral cortex. *Microcirculation* 13, 1–18.
- Čebašek, V., Eržen, I., Vyhmal, A., Janáček, J., Ribarič, S., Kubínová, L., 2010. The estimation error of skeletal muscle capillary supply is significantly reduced by 3D method. *MVR* 779, 40–46.
- Cimrman, R., Rohan, E., 2010. On identification of the arterial model parameters from experiments ~~applicable:in vivo~~. *Math. Comput. Simulat.* 80, 1232–1245.
- Ding, G., Jiang, Q., Li, L., Zhang, L., Zhang, Z.G., Ledbetter, K.A., Panda, S., Chopp, M., 2008. Magnetic resonance imaging investigation of axonal remodeling and

- angiogenesis after embolic stroke in sildenafil-treated rats. *JCBFM* 28, 1440–1448.
- Dryden, I.L., Koloydenko, A., Zhou, D., 2009. Non-Euclidean statistics for covariance matrices, with applications to diffusion tensor imaging. *Ann. Appl. Stat.* 3, 1102–1123.
- Dorph-Petersen, K.A., Nyengaard, J.R., Gundersen, H.J.G., 2001. Tissue shrinkage and unbiased stereological estimation of particle number and size. *J. Microsc.* 204, 232–246.
- Dumais, J., Shaw, S.L., Steele, Ch.R., Long, S.R., Ray, P.M., 2006. An anisotropic-viscoelastic model of plant cells morphogenesis by tip growth. *Int. J. Dev. Biol.* 50, 209–222.
- Dado, D., Levenberg, S., 2009. Cell-scaffold mechanical interplay within engineering tissue. *Sem. Cell Dev. Biol.* 20, 656–664.
- Emons, A.M.C., Mulder, B.M., 1998. The making of the architecture of the plant cell wall: how cells exploit geometry. *Proc. Natl. Acad. Sci. USA* 95, 7215–7219.
- Giachetti, A., Zanetti, G., 2006. Vascular modeling from volumetric diagnostic data: a review. *CMIR* 2, 415–423.
- Grimberg, L.T., Amaro, E., da Silva, A.V., da Silva, R.E., Sato, J.R., dos Santos, D.D., de Paula Pacheco, S., Heinsen, H., 2009. Improved detection of incipient vascular changes by a biotechnological platform combining post mortem MRI in situ with neuropathology. *J. Neurol. Sci.* 283, 2–8.
- Gardner, J.L., 2010. Is cortical vasculature functionally organized? *NeuroImage* 49, 1953–1956.
- Gensei, 2010. <<http://code.google.com/p/gensei/>>.
- Gutkowski, P., Jensen, E.B., Kiderlen, M., 2004. Directional analysis of digitized three-dimensional images by configuration counts. *J. Microsc.* 216, 175–185.
- Geitmann, A., Ortega, J.K.E., 2009. Mechanics and modelling of plant cell growth. *Trends Plant. Sci.* 14, 467–478.
- Guan, Y., Sherman, M., Calvin, J.A., 2006. Assessing isotropy for spatial point processes. *Biometrics* 62, 119–125.
- Howard, C.V., Reed, M.G., 1998. *Unbiased Stereology. Three-Dimensional Measurement in Microscopy*. Springer, New York.
- Holzappel, G.A., Gasser, T.C., 2001. A viscoelastic model for fiber-reinforced composites at finite strains: continuum basis, computational aspects and applications. *Comput. Method. Appl. Mech.* 190, 4379–4403.
- Holzappel, G.A., 2006. Determination of material models for arterial walls from uniaxial extension tests and histological structure. *J. Theor. Biol.* 238, 290–302.
- Hou, Q., Grijpma, D.W., Feijen, J., 2003. Porous polymeric structures for tissue engineering prepared by a coagulation, compression moulding and salt leaching technique. *Biomaterials* 24, 1937–1947.
- Hutmacher, D.W., 2000. Scaffolds in tissue engineering bone and cartilage. *Biomaterials* 21, 2529–2543.
- Inoue, K., 2010. A new approach to the quantitative analysis of the vascular architecture and its application to the cerebral cortex of the reeler mouse. *Hokkaido J. Med. Sci.* 65, 493–509.
- Janáček, J., Cebasek, V., Kubínová, L., Ribarič, S., Erzen, I., 2009. 3D visualization and measurement of capillaries supplying metabolically different fiber types in the rat extensor digitorum longus muscle during denervation and reinnervation. *J. Histochem. Cytochem.* 57, 437–447.
- Jirkovská, M., Kubínová, L., Janáček, J., Moravcová, M., Krejčí, V., Karen, P., 2002. Topological properties and spatial organization of villous capillaries in normal and diabetic placentas. *J. Vasc. Res.* 39, 268–278.
- Jirkovská, M., Janáček, J., Kaláb, J., Kubínová, L., 2008. Three-dimensional arrangement of the capillary bed and its relationship to microrheology in the terminal villi of normal term placenta. *Placenta* 29, 892–897.
- Josso, B., Burton, D.R., Lalor, M.J., 2005. Texture orientation and anisotropy calculation by Fourier transform and principal component analysis. *Mech. Syst. Signal Process.* 19, 1152–1161.
- Kiselev, V.G., Stricker, R., Ziyeh, S., Speck, O., Hennig, J., 2005. Vessel size imaging in humans. *Magnet. Reson. Med.* 53, 553–563.
- Konerding, M.A., Miodonski, A.J., Lametschwandner, A., 1995. Microvascular corrosion casting in the study of tumor vascularity: a review. *Scanning Microsc.* 9, 1233–1243.
- Kubínová, L., Janáček, J., Ribarič, S., Cebasek, V., Erzen, I., 2001. Three-dimensional study of the capillary supply of skeletal muscle fibres using confocal microscopy. *J. Muscle Res. Cell. Motil.* 22, 217–227.
- Kubínová, L., Janáček, J., 2001. Confocal microscopy and stereology: estimating volume, number, surface area and length by virtual test probes applied to three-dimensional images. *Microsc. Res. Tech.* 53, 425–435.
- Kärkkäinen, S., Jensen, E.B.V., 2001. Estimation of fibre orientation from digital images. *Image Anal. Stereol.* 20, 199–202.
- Kiderlen, M., Pfrang, A., 2005. Algorithms to estimate the rose of directions of a spatial fibre system. *J. Microsc.* 219, 50–60.
- Kachlik, D., Baca, V., Stingl, J., 2010. The spatial arrangement of the human large intestinal wall blood circulation. *J. Anat.* 216, 335–343.
- Kiderlen, M., Jensen, E.B.V., 2003. Estimation of the directional measure of planar random sets by digitization. *Adv. Appl. Probab.* 35, 583–602.
- Kochová, P., Cimrman, R., Rohan, E., 2009. Orientation of smooth muscle cells with application in mechanical model of gastropod tissue. *ACM* 3, 75–86.
- Kim, S.-S., Park, M.S., Jeon, O., Choi, Ch.Y., Kim, B.-S., 2006. Poly(lactide-co-glycolide)/hydroxyapatite composite scaffolds for bone tissue engineering. *Biomaterials* 27, 1399–1409.
- Lametschwandner, A., Minnich, B., Kachlik, D., Setina, M., Stingl, J., 2004. Three-dimensional arrangement of the vasa vasorum in explanted segments of the aged human great saphenous vein: scanning electron microscopy and

- three-dimensional morphometry of vascular corrosion casts. *Anat. Rec. A Discov. Mol. Cell. Evol. Biol.* 281, 1372–1382.
- Lametschwandtner, A., Minnich, B., Stöttinger, B., Krautgartner, W.D., 2005. Analysis of microvascular trees by means of scanning electron microscopy of vascular casts and 3D-morphometry. *Ital. J. Anat. Embryol.* 110, 87–95.
- Lim, J.Y., Donahue, H.J., 2007. Cell sensing and response to micro- and nanostructured surfaces produced by chemical and topographic patterning. *Tissue Eng.* 13, 1879–1891.
- Lux, J., Delisée, Ch., Thribault, X., 2006. 3D characterization of wood based fibrous materials: an application. *Image Anal. Stereol.* 25, 25–35.
- Lhotáková, Z., Albrechtová, J., Janáček, J., Kubínová, L., 2008. Advantages and pitfalls of using free-hand sections of frozen needles for three-dimensional analysis of mesophyll by stereology and confocal microscopy. *J. Microsc.* 232, 56–63.
- Monson, K.L., Barbaro, N.M., Manley, G.T., 2008. Biaxial response of passive human cerebral arteries. *Ann. Biomed. Eng.* 36, 2028–2041.
- Mathieu, L.M., Mueller, T.L., Bourban, P.-E., Pioletti, D.P., Müller, R., Manson, J.-A.E., 2006. Architecture and properties of anisotropic polymer composite scaffolds for bone tissue engineering. *Biomaterials* 27, 905–916.
- Mecke, J., 1981. Formulas for stationary planar fibre processes: III. *Intersections with fibre systems.* *Statistics* 12, 201–210.
- Mattfeld, T., 2005. Explorative statistical analysis of planar point processes in microscopy. *J. Microsc.* 220, 131–139.
- Mathieu, O., Cruz-Orive, L.-M., Hoppeler, H., Weibel, E., 1983. Estimating length density and quantifying anisotropy in skeletal muscle capillaries. *J. Microsc.* 131, 131–146.
- Mayhew, T.M., Jairam, I.C., 2000. Stereological comparison of 3D spatial relationships involving villi and intervillous pores in human placentas from control and diabetic pregnancies. *J. Anat.* 197, 263–274.
- Mayhew, T.M., Lucocq, J.M., Griffiths, G., 2002. Relative labelling index: a novel stereological approach to test for non-random immunogold labelling of organelles and membranes on transmission electron microscopy thin sections. *J. Microsc.* 205, 153–164.
- Mayhew, T.M., Mühlfeld, Ch., Vanhecke, D., Ochs, M., 2009. A review of recent methods for efficiently quantifying immunogold and other nanoparticles using TEM sections through cells, tissues and organs. *Ann. Anat.* 191, 153–170.
- PubMed, 2010. <http://www.ncbi.nlm.nih.gov/pubmed, viewed 2010/11/16>.
- Park, S.-H., Masamoto, K., Hendrich, K., Kanno, I., Kim, S.-G., 2008. Imaging brain vasculature with BOLD microscopy: MR detection limits determined by in vivo two-photon microscopy. *Magnet. Reson. Med.* 59, 855–865.
- Prokešová, M., 2003. Bayesian MCMC estimation of the rose of directions. *Kybernetika* 39, 703–717.
- Press, W.H., Teukolsky, S.A., Vetterling, W.T., Flannery, B.P., 1992. *Numerical Recipes in C, The Art of Scientific Computing, 2nd ed.* Cambridge University Press, Cambridge.
- Python, 2001. <http://www.python.org/>.
- Pruyne, D., Bretscher, A., 2000. Polarization of cell growth in yeast. I. Establishment and maintenance of polarity states. *J. Cell Sci.* 113, 365–375.
- Rataj, J., Saxl, I., 1989. Analysis of planar anisotropy by means of the steiner compact. *J. Appl. Probab.* 26, 460–503.
- Romeis, B., 1989. *Mikroskopische Technik.* Urban & Schwarzenberg, München.
- Rieder, M.J., O'Drobinak, D.M., Greene, A.S., 1995. A computerized method for determination of microvascular density. *MVR* 49, 180–189.
- Ranucci, C.S., Kumar, A., Batra, S.P., Moghe, P.V., 2000. Control of hepatocyte function on collagen foams: sizing matrix pores toward selective induction of 2-D and 3-D cellular morphogenesis. *Biomaterials* 21, 783–793.
- Schlimper, C., Nemitz, O., Dorenbeck, U., Scorzin, J., Whitaker, R., Tasdizen, T., Rumpf, M., Schaller, K., 2010. Restoring three-dimensional magnetic resonance angiography images with mean curvature motion. *Neuro. Res.* 32, 87–93.
- Schlageter, K.E., Molnar, P., Lapin, G.D., Groothuis, D.R., 1999. Microvessel organization and structure in experimental brain tumors: microvessel populations with distinctive structural and functional properties. *Microvasc. Res.* 58, 312–328.
- Salu, K.J., Knaapen, M.W.M., Bosmans, J.M., Vrints, Ch.J., Bult, H., 2002. A three-dimensional quantitative analysis of restenosis parameters after balloon angioplasty: comparison between semi-automatic computer-assisted planimetry and stereology. *J. Vas. Res.* 39, 437–446.
- Spodarev, E., 2001. On the rose of intersections of stationary flat processes. *Adv. App. Prob.* 33, 584–599.
- Spodarev, E., 2003. Isoperimetric problems and roses of neighborhood for stationary flat processes. *Math. Nachr.* 251, 88–100.
- Stoyan, D., Kendall, W.S., Mecke, J., 1996. *Stochastic Geometry and its Applications, 2nd ed.* John Wiley & Sons Ltd, New York.
- Sundararaghavan, V., Zabarav, N., 2004. A dynamic material library for the representation of single-phase polyhedral microstructures. *Acta Mater.* 52, 4111–4119.
- Standing, S. (Ed.), 40th ed. Elsevier Churchill Livingstone, Philadelphia (Chapter 15).
- Tonar, Z., Kochová, P., Cimrman, R., Witter, K., Janáček, J., Rohan, V., 2011. Microstructure oriented modelling of hierarchically perfused porous media for cerebral blood flow evaluation. *Key Eng. Mater.* 465, 286–289.
- Tunak, M., Linka, A., 2007. Analysis of planar anisotropy of fibre systems by using 2D Fourier transform. *Fibres Text. East. Eur.* 15, 86–90.
- Wejrzanowski, T., Spychalski, W., Różniatowski, K., Kurzydłowski, K., 2008. Image based analysis of complex microstructures of engineering materials. *Int. J. Appl. Math. Comput. Sci.* 18, 33–39.